THE JOURNAL OF PHYSICAL CHEMISTRY B
A JOURNAL OF THE AMERICAN CHEMICAL SOCIETY

pubs.acs.org/JPCB

Article

# Direct Measurement of Polymer-Chain-End-to-End Distances by Using RAFT Chain Transfer Agent as the FRET Acceptor

*Published as part of The Journal of Physical Chemistry virtual special issue "Early-Career and Emerging Researchers in Physical Chemistry Volume 2".*

Yuming Wang, Alexander W. Fortenberry, Wenlin Zhang, Yoan C. Simon,* and Zhe Qiang*

Cite This: *J. Phys. Chem. B* 2023, 127, 3100−3108

Read Online

ACCESS | Metrics & More | Article Recommendations | Supporting Information

**ABSTRACT:** Förster resonance energy transfer (FRET) is a powerful tool for measuring distances between two molecules (donor and acceptor) in close proximity (1−10 nm), which can be employed for determining polymer end-to-end distances ($R_{ee}$). However, previous works for labeling FRET pairs on chain-ends often involve relatively complex steps for materials preparation, potentially limiting their broad use in synthetic polymer systems. In this work, we introduce an anthracene-functionalized chain-transfer agent for reversible addition−fragmentation chain-transfer (RAFT) polymerizations, which can directly yield polymers containing FRET donor and acceptor molecules on respective chain-ends. This approach enables the direct use of FRET for characterizing the averaged $R_{ee}$ of polymers. Building on this platform, we investigate the averaged $R_{ee}$ of polystyrene (PS) and poly(methyl methacrylate) (PMMA) in a good solvent as a function of their molecular weight. Notably, the FRET results show good agreement with simulation results obtained from all-atom molecular dynamics, confirming its measurement accuracy. Overall, this work provides a facile and broadly applicable platform to directly determine the $R_{ee}$ of low molecular weight polymers by using FRET-based methods.

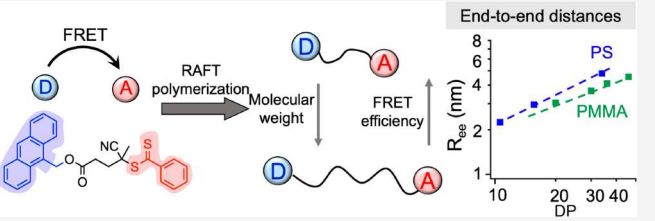


## 1. INTRODUCTION

The conformation of polymer chains can have a profound influence on determining their macroscopic properties.[1−3] For example, in polymer thin films, confinement effects may lead to altered chain conformations due to reduced pervaded volume,[4] resulting in a decreased number of interchain entanglements and distinct mechanical performance compared to their bulk analogs.[5−8] Additionally, kinetic trapping of polymer chains in nonequilibrium states (e.g., through rapid solvent removal) represents an important strategy to enable tunable material properties that are determined by their processing pathways and microstructures.[9−11] Therefore, understanding chain conformations is fundamentally important for controlling polymer properties and informing their rational design and use in many practical applications, such as microelectronics,[12] drug delivery,[13] and nanocomposites.[14]

In general, scattering-based methods, including X-ray,[15] neutron,[16] and light scattering,[17] are commonly employed to study polymer conformations in solution.[18] Specifically, X-ray and neutron scattering give reciprocal space data over a relatively large sample volume. Through accurate model fitting, key physical parameters about polymer single chain behaviors, such as persistence length and contour length, can be extracted. Alternatively, by measuring the light scattering intensity of polymer solutions as a function of their concentration, the radius of gyration ($R_g$) of polymers can be extrapolated via Zimm analysis.[19] While these measurements can provide information about the $R_g$, the end-to-end distances ($R_{ee}$) of polymer chains are usually more difficult to directly access from experiments. Furthermore, most experimental investigations about polymer chain conformations have focused on high molecular weight systems (e.g., >10 000 Da),[20] due to the challenges of obtaining reliable scattering measurements from polymers with small characteristic dimensions (i.e., $R_g$ < 2 nm). To address this challenge, Scherk et al. employed double electron−electron resonance spectroscopy (DEER) to determine the $R_{ee}$ of low molecular weight polymers, using poly(ethylene oxide) (PEO) as a model system.[21] DEER characterizes the dipole−dipole interactions and subsequent spin relaxations of labeled functional end-groups.[22] This method enables the measurement of intramolecular distances within a range of 2−9 nm

**Received:** March 13, 2023
**Revised:** March 16, 2023
**Published:** March 28, 2023

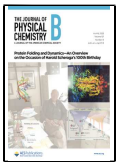

Downloaded via UNIV OF SOUTHERN MISSISSIPPI on February 4, 2024 at 00:21:38 (UTC).
See https://pubs.acs.org/sharingguidelines for options on how to legitimately share published articles.


© 2023 American Chemical Society

https://doi.org/10.1021/acs.jpcb.3c01703
*J. Phys. Chem. B* 2023, 127, 3100−3108

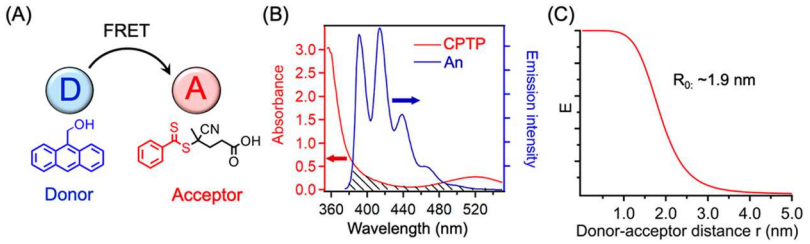


**Figure 1.** (A) Schematic illustration of the FRET mechanism and the chemical structures of donor and acceptor molecules used in this study. (B) UV−vis absorption spectrum of 1 mg/mL CPTP toluene solution (red) and fluorescence emission spectrum (blue) of $10^{-3}$ mg/mL An in toluene solution with an excitation wavelength of 365 nm. The spectral overlap is shaded. (C) The $R_0$ of An/CPTP FRET pair is approximately 1.9 nm, and the relationship of FRET efficiency as a function of An/CPTP pair distance was plotted.

while providing an additional advantage of elucidating the probability distributions of polymer $R_{ee}$.

Förster resonance energy transfer (FRET) is a common tool in biology and life sciences for measuring the conformation of biomacromolecules, such as DNA and proteins.[23−27] Briefly, FRET is a fluorescence-based process, relying on nonradiative energy transfer between two molecules, which are often referred to as donor−acceptor pairs.[28,29] Specifically, the energy transferred from the donor to the acceptor molecules is based on Coulombic interaction through resonance. Key requirements for FRET to occur include (1) spectral overlap between donor emission and acceptor absorption and (2) sufficient physical proximity between the FRET pair, typically in the range of 1−10 nm (Figure 1). The efficiency of FRET is distance-dependent, allowing their use to measure the proximity between donor and acceptor molecules.[30−33] Particularly, when a FRET pair is attached on the same molecule, intramolecular distances, structures, and dynamics can be elucidated.[34−37] However, compared to the field of life science, FRET applications remain underexplored in synthetic polymer systems to study $R_{ee}$.[38−40] Qin et al. prepared anthracene (An)- and carbazole-labeled polystyrene (PS) and poly(methyl methacrylate) (PMMA), through the combined use of atom-transfer radical polymerization (ATRP) and azide−alkyne click chemistry.[41] In their work, FRET was employed to reveal how polymer solution concentration impacts their conformations. Similarly, intramolecular FRET was used to understand the conformation of polymer chains that are chemically grafted onto a planar quartz substate, as a function of their swelling degree under different solvent environments.[42] In most cases, labeling polymer chains with a FRET pair requires multiple synthesis steps, e.g., postpolymerization functionalization and extensive purification, which can be time-consuming and challenging with low coupling efficiency.

Reversible addition−fragmentation chain-transfer (RAFT) polymerization is widely employed to synthesize polymers with defined molecular weight and low dispersity ($Đ$).[43,44] In RAFT, chain-transfer agents (CTAs) effectively suppress radical−radical coupling-terminations during polymerizations. Conveniently, many CTAs absorb light in both the UV and visible light range, owing respectively to a $\pi-\pi^*$ transition and to a forbidden $n-\pi^*$ transition,[45] which may be leveraged to quench the emission of fluorophores that are in close proximity.[46] For example, PS that contains An and dithiobenzoate moieties on respective chain-ends shows an enhanced fluorescence intensity with increased degree of polymerization (DP), confirming that energy transfer between An and CTA is distance-dependent, while suggesting that CTAs can serve as FRET acceptors.[46] However, the ability of using FRET to determine the relationship between energy transfer efficiency and polymer $R_{ee}$ was not presented.

In this work, we leveraged RAFT polymerization to prepare several $\alpha,\omega$-heterotelechelic PS and PMMA polymers flanked with An (donor) and a dithiobenzoate CTA (acceptor). Depending on their proximity, the CTA is able to quench An emission fluorescence, the two acting as a "spectroscopic ruler", whereby FRET efficiency is used to quantify the $R_{ee}$ of the chains. Using this approach, we systematically determine the $R_{ee}$ of a series of PS and PMMA samples, with different molecular weight ranging from 1600 to 5100 Da. Moreover, we compared these results with all-atom molecular dynamics (MD) simulations to assess the accuracy of FRET measurements as well as the impact of end-groups (the FRET pair). Gratifyingly, our system can yield high labeling efficiency without involving any postpolymerization functionalization step to label the chains, which significantly streamlines materials preparation, potentially allowing the broad use of FRET method in the polymer community.

## 2. METHODS

**2.1. Materials.** Methyl methacrylate (MMA, 99%), styrene (99%), 4-cyano-4-(phenylcarbonothioylthio)pentanoic acid (CPTP), 2,2′-azobis(2-methylpropionitrile) (AIBN), hexane (HPLC grade), tetrahydrofuran (THF, 99%), methanol (99%), dichloromethane (DCM, 99.8%), *N*,*N*′-dicyclohexylcarbodiimide (DCC, 99%), 4-*N*,*N*-dimethylaminopyridine (DMAP, 99%), deuterated chloroform ($CDCl_3$, 99.8 atom % D), and 9-anthracenemethanol (An-OH, 97%) were purchased from Sigma-Aldrich. Toluene (HPLC grade) was obtained from Fisher Chemical. Both MMA and styrene monomers were purified via column adsorption using basic aluminum oxide (Sigma-Aldrich) in order to remove inhibitors (monomethyl ether hydroquinone). All other chemicals were used as received.

**2.2. Synthesis of Anthracene Functionalized CTA (An-CPTP).** A typical procedure for the preparation of An-CPTP is as follows: In a 50 mL round-bottom flask (RBF) at 0 °C (ice bath), CPTP (0.3 g, 0.001 mol), An-OH (0.39 g, 0.00185 mol), and DMAP (0.1 g, 0.0008 mol) were first added to anhydrous DCM (20 mL) and stirred for 10 min. DCC (0.66 g, 0.003 mol) was dissolved into DCM (4 mL) and added dropwise to the solution over 20 min. The solution was warmed to room temperature and stirred overnight. Subsequently, the mixture was dried under reduced pressure using a Büchi Rotavapor R-205 rotary evaporator. The product (An-CPTP) was purified via flash chromatography (Teledyne Isco CombiFlash with RediSep Rf prepacked columns) using a


https://doi.org/10.1021/acs.jpcb.3c01703
J. Phys. Chem. B 2023, 127, 3100−3108

mixture of hexane and DCM (40:60 v/v; $R_f$ = 0.35). The fractions were collected and dried under vacuum in a vacuum oven for 12 h. The final product was a red solid.

**2.3. Synthesis of Polymers Using An-CPTP.** A typical procedure of preparing polymers using An-CPTP is as follows: To a 10 mL RBF, MMA (0.41 g, 4.1 mmol), An-CPTP (20.4 mg, 0.051 mmol), and AIBN (1.4 mg, 0.0085 mmol) were introduced to toluene (3.61 mL) (target $M_n$ = 10 000 Da), and the mixture was degassed with $N_2$ (purity >99.99%) for 15 min in order to remove residual oxygen. The polymerizations were conducted at 75 °C under constant agitation for different amounts of time (ranging from 1 to 8 h). Subsequently, the reaction solution was cooled down to room temperature and concentrated by gently blowing $N_2$ over the solution surface. The concentrated solution was then precipitated into methanol (~100 mL) to obtain solids. The precipitate was collected by gravity filtration and dried under vacuum in a vacuum oven for 12 h. For the synthesis of PS, a similar procedure (as described above) was employed while the reaction was conducted at 100 °C for different times, using styrene as the monomer and with the same target molecular weight of $M_n$ = 10 000 Da.

**2.4. End-Group Removal of Synthesized PMMA.** In a 10 mL RBF, 60 mg of synthesized PMMA ($M_n$ = 4100 Da) and 56 mg of AIBN (20 molar time excess) were added to 5 mL of toluene. The mixture was purged with $N_2$ for 15 min to remove oxygen species. Subsequently, the solution was heated to 85 °C under $N_2$ protection for 4 h. The reaction solution was then cooled down to room temperature and concentrated by gently blowing $N_2$ over the solution surface. The concentrated solution was then precipitated into cold methanol to obtain solids. The precipitate (white solids) was collected by gravity filtration and dried under vacuum in a vacuum oven for 12 h.

**2.5. Sample Characterization.** Gel permeation chromatography (GPC) results of polymer samples were obtained using a TOSOH EcoSEC HLC-8320 GPC equipped with TSKgel SuperMultiPore HZ-M. The instrument was calibrated using a linear calibration against a series of PS standards—PStquick MP-M polystyrene standard. All experiments were conducted at 40°C. The mobile phase was freshly distilled THF with a flow rate of 1.0 mL/min. Sample concentrations were 3 mg/mL in THF, and the injection volume was 10 $\mu$L. Conversion of polymerization was determined by calculating the ratio of $M_n$ determined by GPC measurements and target $M_n$. Nuclear magnetic resonance (NMR) spectroscopy was performed with a Bruker 400 MHz NMR, and the sample concentrations were approximately 10−25 mg/mL in $CDCl_3$. $^1$H NMR spectroscopy measurements were performed with 32 proton scans and proton relaxation delays of 5 s for An-CPTP and 64 proton scans with proton relaxation decays of 5s for polymer samples. $^{13}$C NMR measurement was performed with 512 proton scans and proton relaxation delays of 5 s for An-CPTP. Baseline corrections of NMR spectra were performed using VNMR 6.1C software. Electrospray ionization time-of-flight (ESI TOF) mass spectroscopy was performed with an Agilent 6230 ESI TOF. UV−vis absorption spectra of all samples (with a typical concentration of 0.3 mg/mL) were recorded at room temperature in toluene using a PerkinElmer Lambda 35 UV/vis spectrometer.

Steady-state fluorescence measurements were recorded using a PTI-Horiba QuantaMaster 400 spectrofluorometer equipped with a 75 W Xe arc lamp. Solution concentration of polymer samples was approximately $10^{-6}$ mol/mL. This concentration was sufficiently dilute to avoid intermolecular FRET to occurr. For normalizing emission intensity, molar concentration of An molecules in solutions was determined by UV−vis spectroscopy. Additionally, the polymer critical overlapping concentration can be determined through an established method,[47] which is estimated to be approximately 0.1−0.2 mg/mL for all samples studied in this work. For An-containing molecules, the excitation wavelength was at 365 nm and the emission spectrum was collected from 380 to 540 nm. For FRET measurements and calculations of $R_{ee}$, $R_0$ (Förster distance) of FRET pair was first determined by the following equation:

$$R_0 = 0.211(\kappa^2 \eta^{-4} Q_D J(\lambda))^{1/6} \tag{1}$$

where $\kappa^2$ is the orientation factor of dipoles, which is 0.67 for a freely rotating donor and acceptor group; $\eta$ is the refractive index for the medium (1.49 for toluene); $Q_D$ is the fluorescence quantum yield of the donor; and $J(\lambda)$ is the spectral overlap integral which measures the extent of spectral overlap between the normalized donor emission $[F_D(\lambda)]$ and the acceptor absorption spectra ($\varepsilon_A$). The equation for determining J($\lambda$) is described as

$$J(\lambda) = \frac{\int_0^\infty F_D(\lambda)\, \varepsilon_A(\lambda)\, \lambda^4\, d\lambda}{\int_0^\infty F_D(\lambda)\, d\lambda} \tag{2}$$

where $\varepsilon_A$ is the extinction coefficient of the acceptor in the unit of $M^{-1}$ $cm^{-1}$, $\lambda$ is the wavelength in nm, and $F_D$ is the wavelength dependent donor emission spectrum normalized to an area of 1. The unit of $J(\lambda)$ is $M^{-1}$ $cm^{-1}$ $nm^4$. Moroever, fluorescence anisotropy of An molecule was determined by obtaining its vertically polarized emission spectra upon excitation by the light that is vertically and horizontally polarized, respectively, as described by

$$r = \frac{I_{VV} - GI_{VH}}{I_{VV} + 2GI_{VH}} \tag{3}$$

where $I_{VV}$ and $I_{VH}$ are the vertically polarized fluorescence emission intensities when the sample is excited with vertically and horizontally polarized light, respectively. $G$ is the grating factor for correcting the instrument's differential transmission of the two orthogonal vector orientations (=1).

The FRET efficiency between donor and acceptor can be calculated by

$$E = 1 - \frac{I_{DA}}{I_D} \tag{4}$$

where $I_{DA}$ and $I_D$ are the total donor fluorescence emission intensity (normalized with fluorophore concentration) in the presence and absence of A, respectively. The FRET efficiency was then used to determine the average end-to-end distance of polymers, using the following equation:

$$E = \int_{R_{ee,min}}^{R_{ee,max}} p(R_{ee}) \frac{{R_0}^6}{{R_0}^6 + {R_{ee}}^6}\, dR_{ee} \tag{5}$$

where $R_0$ is the Förster distance of donor and acceptor pair, $R_{ee}$ is the average end-to-end distance of polymer chains, and $p(R_{ee})$ follows the flexible chain model as shown below.[48]

$$p(R_{ee}) = 4\pi r^2 \left(\frac{3}{2\pi N b^2}\right)^{3/2} \exp\left(-\frac{3}{2}\frac{{R_{ee}}^2}{Nb^2}\right) \tag{6}$$



https://doi.org/10.1021/acs.jpcb.3c01703
J. Phys. Chem. B 2023, 127, 3100−3108

where $N$ is the total amounts of the chain segments and $b$ is the Kuhn length of polymer chains.

**2.6. Simulation Methods for Determining Polymer Chain $R_{ee}$.** To validate the FRET method, we employed all-atom MD simulations to characterize polymer-chain-end-to-end distances as a function of molecular weight for syndiotactic and isotactic PMMA and PS in toluene solutions. The polymer chains and the solvents were modeled using the OPLS (optimized potentials for liquid simulations) force field, which was optimized for organic liquids, including conventional polymers and solvents.[49,50] In our simulations, polymer chains of various lengths were relaxed in boxes containing 1200 toluene molecules. To ensure the dilute solution condition, the number of polymers was decreased from 20 to 4 as the DP increased from 10 to 36, which correspond to counter lengths ranging from 2.5 to 9 nm. We only simulated PMMA and PS oligomers to keep the computational expense manageable; simulating atactic chains in the MD simulations is not feasible due to the limited length and number of polymer chains. This DP range was also relevant to our experimental work. By simulating both syndiotactic and isotactic chains, our work here represented the boundaries of the conformational phase spaces for atactic PMMA and PS.

The initial configurations of our simulations were obtained by randomly inserting and loosely packing polymer chains and solvent molecules into boxes of a size of $6.5 \times 6.5 \times 6.5$ nm$^3$. The topology files containing all the force field parameters were generated using the LigParGen and PolyParGen servers.[51] We then used the GROMACS package to densify the polymer solutions under the *NPT* condition (refers to constant-temperature, constant-pressure ensemble) at 1 bar and 300 K until the box sizes fluctuated about $6.1 \times 6.1 \times 6.1$ nm$^3$. To confirm that polymers were equilibrated in our simulations, we computed the autocorrelation time for the chain-end-to-end vectors, which characterized the conformational relaxation time for polymer chains. Isotactic PMMA with 36 repeating units had the longest relaxation time, which was about 47 ns. Therefore, by performing additional simulation time of 100 ns, we ensure the equilibration of polymer chains has been reached before data collection. After equilibration, we measured polymer end-to-end vectors $\vec{R}_{ee}$ from *NPT* simulations at a much longer time than the polymer relaxation time. The data collection time for polymers with various DPs ranged from 50 to 800 ns. For each polymer solution, we measured at least 68 independent measurements of $\vec{R}_{ee}$, from which the averaged $R_{ee}$ was obtained.

## 3. RESULTS AND DISCUSSION

Figure 1(A) illustrates the use of FRET for determining polymer chain conformations, employing An as donor and CPTP as acceptor. The energy transfer efficiency between these two molecules is dependent on their physical proximity and Förster distance. Specifically, An can be excited at 365 nm, resulting in a fluorescence emission spectrum that spans from 375 to 540 nm, while CPTP exhibits a $\pi-n^*$ absorption peak in the range of 440 to 550 nm with a molar absorption coefficient of 168 M$^{-1}$ cm$^{-1}$. Figure 1B shows the spectral overlap between An emission and CPTP absorption which enables them to be an effective FRET donor−acceptor pair (extended range of CPTP absorption spectrum from 290 to 700 nm is provided in Figure S1). Using eq 2, we determined that the $J(\lambda)$ of this pair is $1.19 \times 10^{13}$ M$^{-1}$ cm$^{-1}$ nm$^4$. The spectral overlap, sufficiently high quantum yield of the donor fluorophore, and close proximity of the pairs are key requirements for FRET. We used eq 1 to determine the Förster distance ($R_0$) of An/CPTP pair, which is approximately 1.9 nm. Herein, the quantum yield of An molecules in toluene is approximately 0.29, while $\kappa^2$ of 0.67 was used as a good estimate since An molecules have a very low reorientation time and anisotropy value.[52,53] To further confirm that chemical attachment of An onto CPTP and polymer chains does not alter its fluorescence anisotropy value, additional experiments were performed. As shown in Figure S2, fluorescence anisotropy of An, An-CPTP, and An-containing polymers is 0.06, 0.06, and 0.05, respectively, indicating the near isotropic nature of An even as they are covalently linked to CPTP and polymers. The result of An fluorescence anisotropy value is also consistent with many previous reports.[54,55] Moreover, we note that the Förster distance of An/CPTP is comparable with previous reports using An/carbazole and An/naphthalene FRET pair, with reported $R_0$ values of 2.3 nm [56] and 1.9 nm, respectively.[57,58] Figure 1C shows the relationship between FRET efficiency and donor−acceptor distance using eqs 4−6), in which the $p(r)$ of a flexible polymer chain model is taken into account. This consideration is important for accurately determining the averaged end-to-end distance of polymers using the FRET method.

A noteworthy advantage of our approach for studying chain dimensions through FRET is the significantly streamlined and simplified process for materials preparation, without the postpolymerization functionalization nor additional purification steps. Herein, we first reacted CPTP with 9-anthracenemethanol via Steglich esterification (Figure 2A),

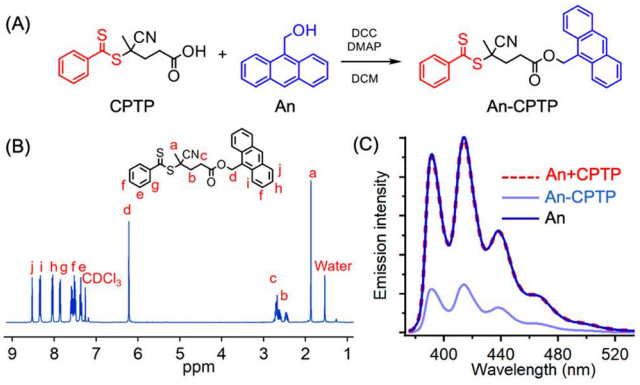


**Figure 2.** (A) Reaction scheme of preparing An-CPTP using Steglich esterification. (B) NMR spectrum of An-CPTP and (C) fluorescence emission spectra of An, An-CPTP, and An/CPTP blend, all in toluene solutions at a concentration of $10^{-3}$ mg/mL. The emission intensity is normalized by the molar concentration of An.

which directly yielded the desired An-functionalized CTA (An-CPTP) for RAFT polymerization. In $^1$H NMR spectroscopy, the marked shift of the methylene peak $\alpha$ to the aromatic group (Figure 2B, 2*H*) from 5.68 to 6.11 ppm indicates the successful esterification between An and CPTP. A detailed analysis including the peak integrations of NMR results as well as the $^{13}$C NMR spectrum of An-CPTP is provided in Figure S3. The mass spectrometry data in Figure S4 also confirm the successful synthesis of An-CPTP with molar masses that match with their predicted values. Figure 2C shows the normalized (based on An molar concentration) fluorescence spectrum of


https://doi.org/10.1021/acs.jpcb.3c01703
J. Phys. Chem. B 2023, 127, 3100−3108

An-CPTP, An, and a mixture of An and CPTP (An/CPTP, a physical blend) in toluene solution. For An-CPTP, the emission intensity of An decreased by 75% on account of covalent linking to CPTP. Based on eq 3, it can be determined that the distance between An and dithiobenzoate moiety is approximately 1.7 nm, which is close to the theoretical estimation through bond angle/distance calculations. As a comparison, when physically blending CPTP and An in the solution, the fluorescence emission spectra were nearly identical to that of the An-only solution; i.e., no quenching was observed. Together, these results confirm that the dithiobenzoate moiety must be within a few nanometers to effectively quench An emission via FRET.

Figure 3A depicts the synthesis of donor/acceptor-labeled polymers for FRET measurements, using An-CPTP as the

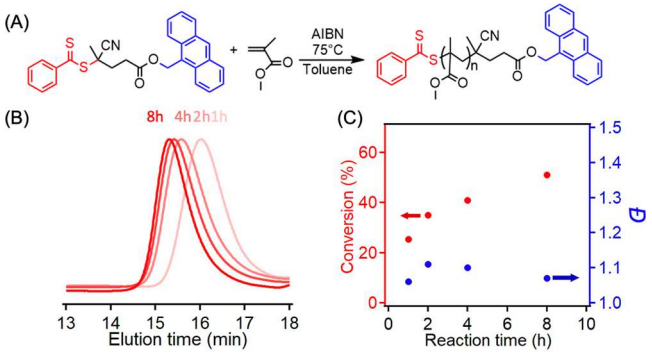


**Figure 3.** (A) Reaction scheme of PMMA synthesis using An-CPTP as the CTA. The monomer concentration in toluene was 1.2 M. (B) GPC traces of as-synthesized PMMA samples from different reaction times. (C) Reaction conversion (determined by $M_n$ obtained from GPC measurements) and polydispersity of PMMA as a function of reaction time.

CTA and MMA as a model monomer. This method directly yields polymers with a FRET pair labeled on the respective chain-ends. Figure 3B shows the GPC results of the as-synthesized PMMA samples, which by increasing the polymerization time, the elution maxima shifted toward shorter times, i.e., higher molecular weights. The monomodal and narrowly distributed traces indicated a well-controlled polymerization process employing An-CPTP as the CTA. Specifically, while increasing the reaction time from 2 to 8 h leads to an increase in the reaction conversion from 22% to 45%, the dispersity ($Đ$) of PMMA samples all remains below 1.15. Additionally, the aromatic signals in the $^1$H NMR spectrum of An-PMMA (Figures S5) confirmed the presence of An and dithiobenzoate moieties on the polymer chains. From the end-group analysis, we found that more than 98% of PMMA contained An and CTA functional groups; this high degree of functionality can be attributed to the relatively low conversion of polymer samples through our RAFT polymerization, where the reactions were quenched in their living state prior to dead chain formations. However, we also want to note that this result indicates that our approach is challenging for resulting in polymers with a perfect 1:1 labeling ratio for donor and acceptor, which is expected from using RAFT polymerization. In this work, An molar concentration of each sample was determined by UV−vis spectroscopy measurement and the Beer−Lamber law,

$$c = \frac{A}{\epsilon l} \tag{7}$$

where $\epsilon$ is the molar extinction coefficient (≈8040 cm$^{-1}$ M$^{-1}$ at 367 nm), $A$ is the absorbance, and $c$ is the molar concentration of An molecules in solution. The obtained molar concentration was then employed for normalizing An emission intensity for the rest of this study. Furthermore, by comparing the polymer averaged end-to-end distances determined from FRET measurements with simulation results in the following section, we can further confirm if this would lead to any significant measurement errors. Similarly, we prepared three PS samples with varying molecular weight from 1600 to 4000 Da. Their GPC traces as a function of reaction time are included in Figure S6, which are monomodal peaks with narrow molecular weight distribution ($Đ$ of all PS samples are below 1.22). These results indicate that An-CPTP can be employed for RAFT polymerizations to prepare PS and PMMA with controlled molecular weight and low polydispersity while enabling the attachment of a FRET pair on respective chain-ends.

The fluorescence emission spectra (normalized with An molar concentration) of PMMA with distinct molecular weight are shown in Figure 4A. It was found that all polymer samples

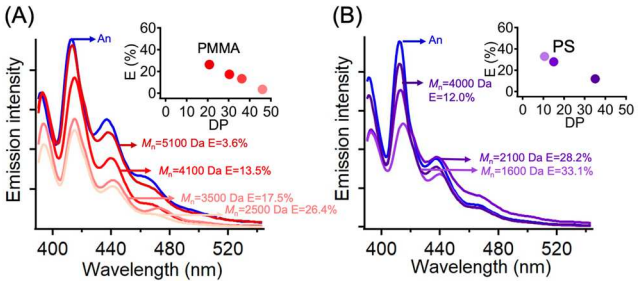


**Figure 4.** Fluorescence emission spectra of (A) PMMA samples and (B) PS samples prepared using An-CPTP as the CTA for RAFT polymerization. The emission intensity was normalized by the molar concentration of An in toluene solution. The excitation wavelength used in this study was 365 nm. FRET efficiency was calculated and plotted as a function of polymer DP, which is provided in the inset of both figures.

exhibited a lower total emission intensity compared to An molecule, which can be attributed to the presence of dithiobenzoate moiety on the polymer end, enabling the FRET process to occur. Among all samples, PMMA with molecular weight of 2500 Da shows the lowest emission intensity, corresponding to a FRET efficiency of 26.4% determined by eq 3. Increasing the molecular weight of PMMA leads to a higher fluorescence emission intensity, indicating the FRET process becomes less efficient. Such changes are anticipated as polymers with higher molecular weight are composed of larger molecule sizes, leading to a longer distance between An and dithiobenzoate groups which are labeled on chain-ends. For PMMA with molecular weight of 5100 Da, a very low FRET efficiency of 3.6% was observed. A similar trend was observed for all PS samples, which are shown in Figure 4B. Specifically, the FRET efficiency of PS samples decreased from 33.1% to 12.0% when the molecular weight increased from 1600 to 4000 Da. The relationship between the FRET efficiency and polymer DP was included in the insets of Figure 4A,B, showing that increasing the DP results in a lower FRET efficiency. To further confirm that the quenching of An fluorescence emission is due to the presence of dithiobenzoate end-group, the CTA moiety was removed


https://doi.org/10.1021/acs.jpcb.3c01703
J. Phys. Chem. B 2023, 127, 3100−3108

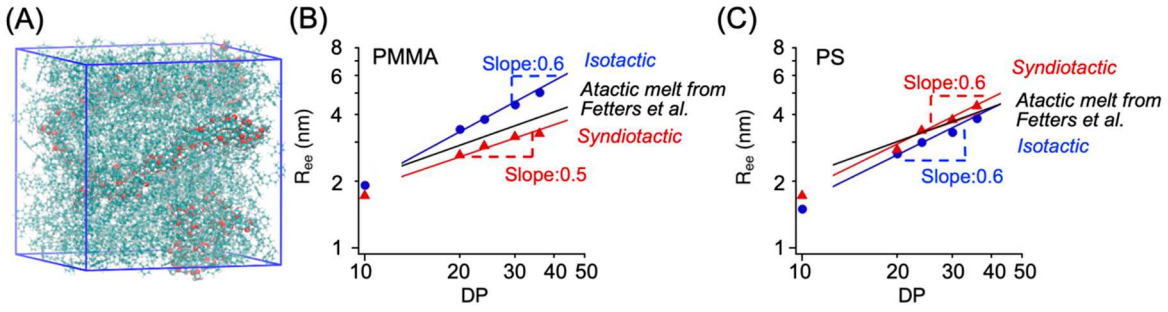


**Figure 5.** (A) A snapshot of four PMMA chains (isotactic, DP = 36) in toluene. Simulation results for syndiotactic and isotactic samples, including (b) $R_{ee}$ as a function of DP for PMMA. (c) $R_{ee}$ as a function of DP for PMMA from simulations. Both (b) and (c) include error bars, which are smaller than symbol size. SANS measurements for $R_{ee}$ of atactic PMMA and PS in melt from Fetters et al.[61] were also included.

from a PMMA sample (molecular weight: 4100 Da) using a radical-based method.[59,60] The disappearance of the absorption peak signal between 440 and 600 nm in UV−vis spectroscopy confirmed the successful removal of the dithiobenzoate (Figure S7). Subsequently, fluorescence measurement of An-functionalized PMMA was performed for samples with the absence of CTA (after the removal of RAFT end-group), showing a nearly complete recovery (~98%) of the An emission intensity in Figure S8. Similarly, a near full recovery of emission intensity was observed for PMMA with lower molecular weights after end group removal. This result confirms that dithiobenzoate moiety is responsible for the quenching of An emission, and the obtained FRET efficiency can be used to characterize the average end-to-end distance of polymers.

To quantitively determine the accuracy of FRET method for measuring polymer $R_{ee}$, we first employed MD simulations (Figure 5A) for obtaining the $R_{ee}$ of PS and PMMA with isotactic and syndiotactic configurations. For PMMA samples, the isotactic samples consistently exhibit a larger $R_{ee}$ than their syndiotactic counterparts. When DP equals 10, the averaged $R_{ee}$ for isotactic and syndiotactic PMMA was found to be 1.9 and 1.7 nm, respectively. As shown in Figure 5B, increasing DP to 36 leads to a more significant $R_{ee}$ difference, in which isotactic PMMA has an averaged $R_{ee}$ of 5 nm while syndiotactic PMMA has an averaged $R_{ee}$ of 3.3 nm. The simulation results for PS samples are shown in Figure 5C, in which the impact of tacticity on polymer conformations is much less obvious than PMMA samples. The syndiotactic PS only shows a slightly higher $R_{ee}$ than their isotactic counterparts. Polymer chain dimensions obtained from our MD simulations in general follow the trends from SANS results of the atactic PS and PMMA samples in melt.[61] Furthermore, when DP was sufficiently large, isotactic and syndiotactic PS and isotactic PMMA behaved as self-avoiding random walks in toluene with $R_{ee} \sim N^{0.6}$.[62] However, syndiotactic PMMA still behaved like ideal Gaussian conformations ($R_{ee} \sim N^{0.5}$) in our simulations, within the molecular weight range of interests (up to 5200 Da). We argue that the excluded volume interactions of syndiotactic PMMA in toluene are weak so that the thermal blob size is greater than the oligomeric chains in our simulations. In other words, the syndiotactic PMMA chains were too short to exhibit self-avoiding statistics.

Using the FRET efficiency results in Figure 4, $R_{ee}$ of PS and PMMA samples can be determined by eqs 4−6. The PMMA sample shows an averaged $R_{ee}$ of 3 nm, 3.7 nm, 4.1 nm, and 4.5 nm, when their molecular weight is 2500 Da, 3500 Da, 4100 Da, and 5100 Da, respectively. A similar trend was observed for PS samples, in which the $R_{ee}$ increases from 2.6 nm (with PS molecular weight of 1600 Da) to 4.3 nm (with PS molecular weight of 4000 Da). The probability of $R_{ee}$ of all PS and PMMA samples is provided in Figure S9. The averaged $R_{ee}$ values resulting from FRET measurements are compared with simulation results, as shown in Figure 6. Since the tacticity was

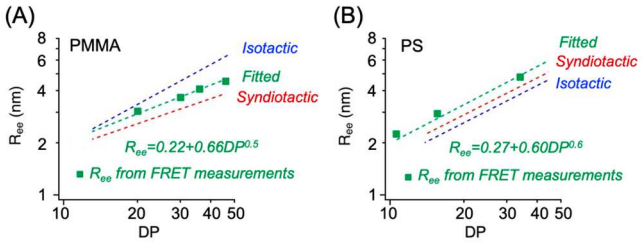


**Figure 6.** Experiment results of $R_{ee}$ from FRET measurements for (A) PMMA and (B) PS samples as a function of degree of polymerization (DP). The fitting functions (using eq 8) are also provided in the figure and compared to simulation results.

not controlled in our RAFT polymerizations, all as-synthesized polymer samples are atactic. For PMMA, our experimental results of their averaged $R_{ee}$ are in between with that of syndiotactic and isotactic samples (obtained from MD simulations) at the same molecular weight. However, the averaged $R_{ee}$ of PS samples determined from FRET measurements is slightly higher than their syndiotactic and isotactic counterparts. We attribute the increased polymer chain sizes to the presence of end-groups, including both An and CTA. This effect is less pronounced for PMMA samples, since their tacticity plays a more significant role in controlling polymer chain sizes. Furthermore, the following equation was used to fit the result of averaged $R_{ee}$ (from FRET measurements) as a function of DP:

$$R_{ee} = a(\mathrm{DP})^{\nu} + b \tag{8}$$

where $a$ is a coefficient depending on monomer chemistry, $\nu$ is a scaling exponent that depends on solvent solubility, and $b$ is a contributing factor on polymer $R_{ee}$ due to the presence of end-groups. As shown in Figure 6, we found that best fitting of $R_{ee}$ as a function of DP was obtained when $\nu$ is 0.5 and 0.6 for PMMA and PS, respectively. Furthermore, it is important to note the fitting function of both PS and PMMA contains a similar intercept $b$, with a value between 0.22 and 0.27, which is associated with the impact of CTA and An molecules on increasing the polymer $R_{ee}$; the presence of end functional


https://doi.org/10.1021/acs.jpcb.3c01703
J. Phys. Chem. B 2023, 127, 3100−3108

groups on altering polymer chain sizes is also reported in other literature examples.[38,63] Additionally, the polydispersity of synthesized polymers may also contribute to the small deviations between experimental and simulation results. We also want to note that fluorescence emission behaviors of An as well as the ability of CPTP to quench its emission could also be potentially influenced by several other factors, such as scattering and UV-absorption of polymers, photobleaching (during synthesis, storage, and measurements), and changes in the electronic environment of An after chemically attaching to polymer chains. Nevertheless, this work demonstrates a facile FRET-based approach to determine the chain conformation of low molecular weight polymers, which uses the CTA as the acceptor and does not require post functionalization and purification steps after polymer synthesis. Building upon this effort, we believe there are opportunities to further combine these FRET systems with fluorescence microscopy for imaging the spatial heterogeneity of chain conformations in solid states, enabling an important characterization platform for polymer community.

## 4. CONCLUSIONS

In this work, we employ a FRET-based method to directly measure polymer end-to-end distances ($R_{ee}$), in which the donor and acceptor molecules are incorporated onto the respective chain-ends. Specifically, anthracene-functionalized CTA is synthesized and used for preparing PS and PMMA through RAFT polymerizations. Energy transfer efficiency between anthracene molecules and dithioester group on the CTA was systematically investigated as a function of molecular weight for both PS and PMMA. The obtained results can then be employed for studying the polymer chain dimensions in solution state, demonstrated by determining polymers $R_{ee}$ in toluene as model systems. We confirm the accuracy of this FRET approach on reporting polymer $R_{ee}$ through performing quantitative comparisons with results obtained from all-atom molecular dynamics simulations. Our method eliminates the postpolymerization functionalization steps for dye/fluorophore labeling, allowing streamlined sample preparations for FRET measurements. We believe this method can also be extended to other fluorophore/CTA molecules as FRET pairs for studying chain conformations of low molecular weight polymers with various chemistry, providing great potential to broadly benefit the polymer physics community.

## ■ ASSOCIATED CONTENT

### Supporting Information

The Supporting Information is available free of charge at https://pubs.acs.org/doi/10.1021/acs.jpcb.3c01703.

$^1$H NMR spectrum, $^{13}$C NMR spectrum, and mass spectrometry results of An-CPTP; $^1$H NMR spectra of PMMA prepared by RAFT polymerization using An-CPTP as the CTA; GPC traces of PS samples, UV−vis and fluorescence emission spectra of PMMA sample before and after the removal of CTA; and p($R_{ee}$) plots of PMMA and PS samples (PDF)

## ■ AUTHOR INFORMATION


### Corresponding Authors

**Yoan C. Simon** − *School of Polymer Science and Engineering, University of Southern Mississippi, Hattiesburg, Mississippi 39406, United States;* orcid.org/0000-0002-5235-6127; Email: yoan.simon@usm.edu

**Zhe Qiang** − *School of Polymer Science and Engineering, University of Southern Mississippi, Hattiesburg, Mississippi 39406, United States;* orcid.org/0000-0002-3539-9053; Email: zhe.qiang@usm.edu

### Authors

**Yuming Wang** − *School of Polymer Science and Engineering, University of Southern Mississippi, Hattiesburg, Mississippi 39406, United States*

**Alexander W. Fortenberry** − *School of Polymer Science and Engineering, University of Southern Mississippi, Hattiesburg, Mississippi 39406, United States*

**Wenlin Zhang** − *Department of Chemistry, Dartmouth College, Hanover, New Hampshire 03755, United States;* orcid.org/0000-0001-6026-4284

Complete contact information is available at: https://pubs.acs.org/10.1021/acs.jpcb.3c01703


### Author Contributions

The manuscript was written through contributions of all authors. All authors have given approval to the final version of the manuscript.

### Notes

The authors declare no competing financial interest.

## ■ ACKNOWLEDGMENTS

This work was partially supported by National Science Foundation Office of Integrative Activities Grants 1757220 and 2132144. Z.Q. also acknowledges financial support provided from ACS Petroleum Research Fund (Award 65268-DNI7). W.Z. also acknowledges ACS Petroleum Research Fund (Award 62491-DNI7) for financial support. Mass spectrometry experiments were performed at the LSU Mass Spectrometry Facility (MSF).

## ■ REFERENCES


(1) Bukowski, C.; Zhang, T.; Riggleman, R. A.; Crosby, A. J. Load-bearing entanglements in polymer glasses. *Sci. Adv.* **2021**, *7*, eabg9763.

(2) Zhang, Y.; Fakhraai, Z. Decoupling of surface diffusion and relaxation dynamics of molecular glasses. *Proc. Natl. Acad. Sci. U.S.A.* **2017**, *114*, 4915−4919.

(3) Noriega, R.; Salleo, A.; Spakowitz, A. J. Chain conformations dictate multiscale charge transport phenomena in disordered semiconducting polymers. *Proc. Natl. Acad. Sci. U. S. A.* **2013**, *110*, 16315−16320.

(4) Sussman, D. M.; Tung, W.-S.; Winey, K. I.; Schweizer, K. S.; Riggleman, R. A. Entanglement reduction and anisotropic chain and primitive path conformations in polymer melts under thin film and cylindrical confinement. *Macromolecules* **2014**, *47*, 6462−6472.

(5) Xia, W.; Hsu, D. D.; Keten, S. Molecular weight effects on the glass transition and confinement behavior of polymer thin films. *Macromol. Rapid Commun.* **2015**, *36*, 1422−7.

(6) Yoshimoto, K.; Jain, T. S.; Nealey, P. F.; de Pablo, J. J. Local dynamic mechanical properties in model free-standing polymer thin films. *J. Chem. Phys.* **2005**, *122*, 144712.

(7) Kropka, J. M.; Pryamitsyn, V.; Ganesan, V. Relation between glass transition temperatures in polymer nanocomposites and polymer thin films. *Phys. Rev. Lett.* **2008**, *101*, 075702.

(8) García, N. A.; Barrat, J.-L. Entanglement reduction induced by geometrical confinement in polymer thin films. *Macromolecules* **2018**, *51*, 9850−9860.

(9) Chandran, S.; Baschnagel, J.; Cangialosi, D.; Fukao, K.; Glynos, E.; Janssen, L. M. C.; Müller, M.; Muthukumar, M.; Steiner, U.; Xu, J.;

Napolitano, S.; Reiter, G. Processing pathways decide polymer properties at the molecular level. *Macromolecules* **2019**, *52*, 7146−7156.
(10) Jin, Y.; Zhang, A.; Wolf, S. E.; Govind, S.; Moore, A. R.; Zhernenkov, M.; Freychet, G.; Arabi Shamsabadi, A.; Fakhraai, Z. Glasses denser than the supercooled liquid. *Proc. Natl. Acad. Sci. U. S. A.* **2021**, *118*, e2100738118.
(11) Barbero, D. R.; Steiner, U. Nonequilibrium Polymer Rheology in Spin-cast Films. *Phys. Rev. Lett.* **2009**, *102*, 248303.
(12) Stoykovich, M. P.; Müller, M.; Kim, S. O.; Solak, H. H.; Edwards, E. W.; de Pablo, J. J.; Nealey, P. F. Directed assembly of block copolymer blends into nonregular device-oriented structures. *Science* **2005**, *308*, 1442−1446.
(13) He, W.; Parowatkin, M.; Mailänder, V.; Flechtner-Mors, M.; Graf, R.; Best, A.; Koynov, K.; Mohr, K.; Ziener, U.; Landfester, K.; et al. Nanocarrier for oral peptide delivery produced by polyelectrolyte complexation in nanoconfinement. *Biomacromolecules* **2015**, *16*, 2282−2287.
(14) Cheng, S.; Bocharova, V.; Belianinov, A.; Xiong, S.; Kisliuk, A.; Somnath, S.; Holt, A. P.; Ovchinnikova, O. S.; Jesse, S.; Martin, H.; Etampawala, T.; Dadmun, M.; Sokolov, A. P. Unraveling the mechanism of nanoscale mechanical reinforcement in glassy polymer nanocomposites. *Nano Lett.* **2016**, *16*, 3630−3637.
(15) Chu, B.; Hsiao, B. S. Small-angle X-ray xcattering of polymers. *Chem. Rev.* **2001**, *101*, 1727−1762.
(16) Sperling, L. H. Characterization of polymer conformation and morphology through small-angle neutron scattering—A literature review. *Polym. Eng. Sci.* **1984**, *24*, 1−21.
(17) Mao, Y.; Liu, K.; Zhan, C.; Geng, L.; Chu, B.; Hsiao, B. S. Characterization of nanocellulose using small-angle neutron, x-ray, and dynamic light scattering techniques. *J. Phys. Chem. B* **2017**, *121*, 1340−1351.
(18) Higgins, J. S.; Stein, R. S. Recent developments in polymer applications of small-angle neutron, x-ray and light Scattering. *J. Appl. Crystallogr.* **1978**, *11*, 346−375.
(19) Chu, B. *Laser Light Scattering: Basic Principles and Practice*; Courier Corporation, 2007.
(20) Le Coeur, C.; Combet, S.; Carrot, G.; Busch, P.; Teixeira, J.; Longeville, S. Conformation of the poly(ethylene glycol) chains in DiPEGylated hemoglobin specifically probed by SANS: Correlation with PEG length and in vivo efficiency. *Langmuir* **2015**, *31*, 8402−8410.
(21) Sherck, N.; Webber, T.; Brown, D. R.; Keller, T.; Barry, M.; DeStefano, A.; Jiao, S.; Segalman, R. A.; Fredrickson, G. H.; Shell, M. S.; et al. End-to-end distance probability distributions of dilute poly(ethylene oxide) in aqueous solution. *J. Am. Chem. Soc.* **2020**, *142*, 19631−19641.
(22) Banham, J. E.; Baker, C. M.; Ceola, S.; Day, I. J.; Grant, G. H.; Groenen, E. J.; Rodgers, C. T.; Jeschke, G.; Timmel, C. R. Distance measurements in the borderline region of applicability of CW EPR and DEER: a model study on a homologous series of spin-labelled peptides. *J. Magn. Reson.* **2008**, *191*, 202−218.
(23) Didenko, V. V. DNA probes using fluorescence resonance energy transfer (FRET): designs and applications. *Bioconjugate Chem.* **2001**, *31*, 1106−1121.
(24) Long, Y.; Ubych, K.; Jagu, E.; Neely, R. K. FRET-based method for direct, real-time measurement of DNA methyltransferase activity. *Bioconjugate Chem.* **2021**, *32*, 192−198.
(25) Woźniak, A. K.; Schröder, G. F.; Grubmüller, H.; Seidel, C. A. M.; Oesterhelt, F. Single-molecule FRET measures bends and kinks in DNA. *Proc. Natl. Acad. Sci. U.S.A.* **2008**, *105*, 18337−18342.
(26) Hellenkamp, B.; Schmid, S.; Doroshenko, O.; Opanasyuk, O.; Kühnemuth, R.; Rezaei Adariani, S.; Ambrose, B.; Aznauryan, M.; Barth, A.; Birkedal, V.; et al. Precision and accuracy of single-molecule FRET measurements—A multi-laboratory benchmark study. *Nat. Methods* **2018**, *15*, 669−676.
(27) Algar, W. R.; Hildebrandt, N.; Vogel, S. S.; Medintz, I. L. FRET as a biomolecular research tool—understanding its potential while avoiding pitfalls. *Nat. Methods* **2019**, *16*, 815−829.
(28) Wu, L.; Huang, C.; Emery, B. P.; Sedgwick, A. C.; Bull, S. D.; He, X.-P.; Tian, H.; Yoon, J.; Sessler, J. L.; James, T. D. Förster Resonance Energy Transfer (FRET)-based small-molecule sensors and imaging agents. *Chem. Soc. Rev.* **2020**, *49*, 5110−5139.
(29) Roy, R.; Hohng, S.; Ha, T. A practical guide to single-molecule FRET. *Nat. Methods* **2008**, *5*, 507−516.
(30) Lai, W.-J. C.; Kayedkhordeh, M.; Cornell, E. V.; Farah, E.; Bellaousov, S.; Rietmeijer, R.; Salsi, E.; Mathews, D. H.; Ermolenko, D. N. mRNAs and lncRNAs intrinsically form secondary structures with short end-to-end distances. *Nat. Commun.* **2018**, *9*, 43281.
(31) Odrobina, E.; Winnik, M. A. Influence of entanglements on the time dependence of mixing in nonradiative energy transfer studies of polymer diffusion in latex films. *Macromolecules* **2001**, *34*, 6029−6038.
(32) Sandoval, R. W.; Williams, D. E.; Kim, J.; Roth, C. B.; Torkelson, J. M. Critical micelle concentrations of block and gradient copolymers in homopolymer: Effects of sequence distribution, composition, and molecular Weight. *J. Polym. Sci. B: Polym. Phys.* **2008**, *46*, 2672−2682.
(33) Major, M. D.; Torkelson, J. M.; Brearley, A. M. Fluorescence energy-transfer studies of bulk styrene-isoprene diblock copolymers and their blends with polyisoprene: Applications to microphase separation. *Macromolecules* **1990**, *23*, 1711−1717.
(34) Qiang, Z.; Wang, M. 100$^{th}$ Anniversary of macrmolecular science viewpoint: Enabling advances in fluorescence microscopy techniques. *ACS Macro Lett.* **2020**, *9*, 1342−1356.
(35) Valdez, S.; Robertson, M.; Qiang, Z. Fluorescence resonance energy transfer measurements in polymer science: A review. *Macromol. Rapid Commun.* **2022**, *43*, 2200421.
(36) Yang, J.; Lou, X.; Spiro, J. G.; Winnik, M. A. Energy transfer study of the cylindrical interface formed by asymmetric isoprene−methyl methacrylate diblock copolymers bearing a dye at the junction. *Macromolecules* **2006**, *39*, 2405−2412.
(37) Merckx, R.; Swift, T.; Rees, R.; Van Guyse, J. F. R.; Schoolaert, E.; De Clerck, K.; Ottevaere, H.; Thienpont, H.; Jerca, V. V.; Hoogenboom, R. Förster resonance energy transfer in fluorophore labeled poly(2-ethyl-2-oxazoline)s. *J. Mater. Chem. C* **2020**, *8*, 14125−14137.
(38) Sha, Y.; Xu, Y.; Qi, D.; Wan, Y.; Li, L.; Li, H.; Wang, X.; Xue, G.; Zhou, D. Synthesis of heterotelechelic $\alpha,\omega$-dye-labeled polymer and energy transfer between the chain-ends. *Macromolecules* **2016**, *49*, 8274−8281.
(39) Chan, N. Y.; Chen, M.; Dunstan, D. E. Elasticity of polymer solutions in couette flow measured by fluorescence resonance energy transfer (FRET). *Eur. Phys. J. E* **2009**, *30*, 37−41.
(40) Roth, P. J.; Haase, M.; Basché, T.; Theato, P.; Zentel, R. Synthesis of heterotelechelic $\alpha,\omega$ dye-functionalized polymer by the RAFT process and energy transfer between the end-groups. *Macromolecules* **2010**, *43*, 895−902.
(41) Qin, L.; Zhao, N.; Sha, Y.; Chen, H.; Li, L.; Zhou, D.; Chen, W.; Xue, G.; Jia, X. Characterization of conformational transition of polymers with low molecular weights in solutions by fluorescence resonance energy transfer. *Polymer* **2020**, *190*, 122217.
(42) Besford, Q. A.; Yong, H.; Merlitz, H.; Christofferson, A. J.; Sommer, J.-U.; Uhlmann, P.; Fery, A. FRET-integrated polymer brushes for spatially resolved sensing of changes in polymer conformation. *Angew. Chem., Int. Ed.* **2021**, *60*, 16600−16606.
(43) Perrier, S. 50th anniversary perspective: RAFT polymerization—A user guide. *Macromolecules* **2017**, *50*, 7433−7447.
(44) Moad, G.; Rizzardo, E.; Thang, S. RAFT polymerization and some of its applications. *Chem. Asian J.* **2013**, *8*, 1634−1644.
(45) Skrabania, K.; Miasnikova, A.; Bivigou-Koumba, A. M.; Zehm, D.; Laschewsky, A. Examining the UV-vis absorption of RAFT chain transfer agents and their use for polymer analysis. *Polym. Chem.* **2011**, *2*, 2074−2083.
(46) Zhou, N.; Lu, L.; Zhu, X.; Yang, X.; Wang, X.; Zhu, J.; Zhou, D. Preparation and characterization of anthracene end-capped polystyrene via reversible addition-fragmentation chain transfer polymerization. *Polym. Bull.* **2006**, *57* (4), 491−498.


https://doi.org/10.1021/acs.jpcb.3c01703
J. Phys. Chem. B 2023, 127, 3100−3108

(47) Ying, Q.; Chu, B. Overlap concentration of macromolecules in solution. *Macromolecules* **1987**, *20*, 362−366.
(48) Schuler, B.; Soranno, A.; Hofmann, H.; Nettels, D. Single-molecule FRET spectroscopy and the polymer physics of unfolded and intrinsically disordered proteins. *Annu. Rev. Biophys* **2016**, *45*, 207−231.
(49) Tatek, Y. B.; Tsige, M. Structural properties of atactic polystyrene adsorbed onto solid surface. *J. Chem. Phys.* **2011**, *135*, 174708.
(50) Li, Z.; Yuan, F.; Fichthorn, K. A.; Milner, S. T.; Larson, R. G. Molecular view of polymer/water interfaces in latex paint. *Macromolecules* **2014**, *47*, 6441−6452.
(51) Dodda, L. S.; Cabeza de Vaca, I.; Tirado-Rives, J.; Jorgensen, W. L. LigParGen Web server: an automatic OPLS-AA parameter generator for organic ligands. *Nucleic Acids Res.* **2017**, *45*, W331−W336.
(52) Jas, G. S.; Wang, Y.; Pauls, S. W.; Johnson, C. K.; Kuczera, K. Influence of temperature and viscosity on anthracene rotational difussion in organic solvents: Molecular dynamics Ssmluation and fluorescnece anisotropy study. *J. Chem. Phys.* **1997**, *107*, 8800.
(53) Pokorná, V.; Vyprachticky, D.; Pecka, J.; Mikeš, F. Time-resolved emission anisotropy of anthracene fluorophore in the backbone of stereoregular poly(methyl methacrylate). *Macrmolecular. Chem. Phys.* **2001**, *202*, 155−162.
(54) Van Damme, J.; Du Prez, F. Anthracene-containing polymer towards high-end applications. *Prog. Polym. Sci.* **2018**, *82*, 92−119.
(55) Laishram, R.; Maitra, U. Energy transfer in FRET pairs in a supramolecular hydrogel template. *Chem. Commun.* **2022**, *58*, 3162−3165.
(56) Tamai, N.; Yamazaki, T.; Yamazaki, I. Two-dimensional excitation energy transfer between chromophoric carbazole and anthracene in Langmuir-Blodgett monolayer Films. *J. Phys. Chem. A* **1987**, *91*, 841−845.
(57) Liu, G.; Guillet, J. Application of the "spectroscopic ruler" to studies of the dimensions of flexible macromolecules. 1. Theory. *Macromolecules* **1990**, *23*, 1388−1392.
(58) Liu, G.; Guillet, J. Application of the spectroscopic ruler to studies of the dimensions of flexible macromolecules. 3. Equation describing the relative diffusion between polymer chain-ends. *Macromolecules* **1990**, *23*, 2969−2973.
(59) Oishi, E.; Takamura, M.; Takahashi, T. Removal of trithiocarbonyl end-group of RAFT-polymerized poly(stearyl acrylate) and effect of the end-group on thermal and structural properties. *Polymers* **2021**, *13*, 4169.
(60) Willcock, H.; O'Reilly, R. K. End-group removal and modification of RAFT polymers. *J. Polym. Sci.* **2010**, *1*, 149−157.
(61) Fetters, L.; Lohse, D.; Richter, D.; Witten, T.; Zirkel, A. *Connection between polymer molecular weight, density, chain dimensions, and melt viscoelastic properties* **1994**, *27*, 4639−4647.
(62) Schäfer, L. *Excluded Volume Effects in Polymer Solutions: As Explained by the Renormalization Group*; Springer Science & Business Media, 2012.
(63) Qin, L.; Li, L.; Sha, Y.; Wang, Z.; Zhou, D.; Chen, W.; Xue, G. Conformational transitions of polymer chains in solutions characterized by fluorescence resonance energy transfer. *Polymers* **2018**, *10* (9), 1007.

## Recommended by ACS

**Dipyrene-Terminated Oligosilanes Enable Ratiometric Fluorescence Response in Polymers toward Mechano- and Thermo-Stimuli**
Guohua Zhu, Yi Li, *et al.*
FEBRUARY 20, 2023
ACS APPLIED MATERIALS & INTERFACES
READ

**"Grafting from" Enabled Stretchable and Highly Fluorescent Carbon Quantum Dot–Polyisoprene Elastomers**
Livy Laysandra, Yu-Cheng Chiu, *et al.*
FEBRUARY 08, 2023
ACS APPLIED POLYMER MATERIALS
READ

**Visualization of the pH Response through Autofluorescent Poly(styrene-*alt*-*N*-maleimide) Polyelectrolyte Brushes**
Gozde Aktas Eken, Christopher Ober, *et al.*
JANUARY 18, 2023
ACS APPLIED POLYMER MATERIALS
READ

**Dual-Color Optical Recording of Bioelectric Potentials by Polymer Electrochromism**
Yuecheng Zhou, Bianxiao Cui, *et al.*
DECEMBER 16, 2022
JOURNAL OF THE AMERICAN CHEMICAL SOCIETY
READ

**Get More Suggestions >**


https://doi.org/10.1021/acs.jpcb.3c01703
*J. Phys. Chem. B* 2023, 127, 3100−3108